# Dynamical model for the interpretation of the geometry of the (4×2) CO layer adsorbed on MgO (001)

C. Girardet, P. N. M. Hoang, and S. Picaud
*Laboratoire de Physique Moléculaire, Faulté des Sciences, Université de Franche–Comté, 25030 Besançon Cedex, France*
(Received 13 December 1995; revised manuscript received 2 February 1996)

A consistent interpretation of the (4×2) CO layer geometry is proposed, which reconciles experimental data obtained from electron diffraction, helium atom scattering, and polarization infrared spectroscopy together with interaction potential calculations. We show that dynamical considerations are required to understand the CO adsorption sites and orientations on the basis of these data. [S0163-1829(96)04923-5]

## I. INTRODUCTION

The adsorption of CO on a clean (001) MgO surface has been among the most studied processes, as it represents a model for physisorption. Low energy electron diffraction[1,2] (LEED) and thermal helium atom scattering[3] (HAS) experiments agree that the stable (sub-) monolayer structure below 40 K is a commensurate $c(4\times2)$ phase, while increasing temperature to 50 K leads to the occurrence of $(1\times1)$ symmetry. From polarization infrared spectroscopy[4,5] (PIRS), two energetically different adsorption sites are expected for CO below 40 K, whereas the high-temperature phase corresponds to equivalent CO dipoles perpendicular to the surface. Inelastic HAS shows,[3] furthermore, one dispersion mode at about 9 meV for the $(1\times1)$ phase and an additional mode at 10.5 meV for the $(4\times2)$ structure, indicating the existence of two inequivalent sites for the admolecules in the second situation.

From examination of these experimental results, one could conclude that the agreement is complete and that these data allow the molecular orientations on the surface to be unambiguously determined. However, a more detailed analysis of these data together with considerations on interaction potential calculations[6] for the determination of stable layer geometry lead us to think that the physical reality could be more complex. In this paper, we summarize the available theoretical results and discuss the stable structures obtained from a minimization procedure of the interaction energy at 0 K. While the most stable structure is unable to account for the infrared features, we show that consideration of angular motions at finite temperature for the admolecules allows the reconciliation of the experimental and theoretical points of view. In Sec. II, we summarize the theoretical backgrounds and we recall, in Sec. III, the previous results issued from static considerations. In Sec. IV, we discuss the influence of the molecular motions and in Sec. V, we interpret the experimental observations from a dynamical point of view.

## II. THEORETICAL BACKGROUNDS

The main part of our theoretical approach has been already discussed elsewhere[2,6,7] and we just recall here the theoretical expressions for the different observables.

### A. The interaction potential

The potentials $V_{\mathrm{MS}}$ and $V_{\mathrm{MM}}$ characterizing, respectively, the monolayer-substrate and the molecule-molecule interactions are described by pairwise atom-atom dispersion-repulsion and electrostatic contributions.

The dispersion-repulsion parts of $V_{\mathrm{MM}}$ and $V_{\mathrm{MS}}$ are written as[8]

$$V_{\mathrm{MM}}^{\mathrm{DR}}=\sum_{k=6,12}\sum_{m,i}\sum_{n,j}(-1)^{k/2}4\epsilon_{ij}\frac{\sigma_{ij}^{k}}{R_{mi,nj}^{k}}, \tag{1}$$

where $R_{mi,nj}$ is the distance between the $i$th atom of molecule $m$ and the $j$th atom of molecule $n$, and

$$V_{\mathrm{MS}}^{\mathrm{DR}}=\sum_{k=6,12}\sum_{m,i}\sum_{\ell,s,p}(-1)^{k/2}4\epsilon_{is}\frac{\sigma_{is}^{k}}{R_{mi,\ell sp}^{k}} \tag{2}$$

$(\ell sp)$ defines the $s$th atom of the $\ell$th primitive cell in the $p$th plane of the substrate. The potential parameters $\epsilon$ and $\sigma$ are given in Table I.

The electrostatic contributions $V_{\mathrm{MM}}^{E}$ and $V_{\mathrm{MS}}^{E}$ come from the interaction between a set of charges, dipoles, and quadrupoles distributed on suitable sites[9] of the adsorbed molecules and the substrate charges. For the adsorbate, this contribution is defined as[8]

$$V_{\mathrm{MM}}^{E}=\sum_{m,i}\sum_{n,j}\sum_{a,b}\underline{M}_{mi}^{a}\underline{T}^{a+b}(\mathbf{R}_{mi,nj})\underline{M}_{nj}^{b}, \tag{3}$$

where $\underline{M}_{mi}^{a}$ represents the $a$th electric multipole moment ($a=0,1,2$ for charge, dipole, and quadrupole, respectively, see Table I) distributed on the $i$th site of molecule $m$. $\underline{T}$ is the usual action tensor of rank $a+b$, which depends on the distance $R_{mi,nj}$. For the interaction between the adsorbate and the substrate charges, one has

$$V_{\mathrm{MS}}^{E}=\sum_{m,i}\sum_{\ell,s,p}\sum_{a}\underline{M}_{mi}^{a}\underline{T}^{a}(\mathbf{R}_{mi,\ell sp})\underline{M}_{\ell sp}^{0}. \tag{4}$$

Other contributions such as higher-order electrostatic terms, induction contribution, corrections terms due to the surface rumpling, etc. remain, in general, weak enough to be disregarded[2] for this system.

Each potential contribution [Eqs. (1)–(4)] depends on the molecule position $(x,y,z)$ and orientation $(\theta,\phi)$ (Fig. 1) and

 

TABLE I. Potential parameters for the molecule-molecule and the molecule-substrate interactions.

| $V^{DR}$ | MS[a] | | | | MM[b] | | |
|---|---|---|---|---|---|---|---|
| | Mg-C | Mg-O | O-C | O-O | C-C | O-O | C-O |
| $\epsilon$ (meV) | 1.51 | 1.6 | 8.1 | 8.64 | 3.72 | 4.64 | 4.16 |
| $\sigma$ (Å) | 3.01 | 2.82 | 3.08 | 2.89 | 3.21 | 2.96 | 3.08 |
| $V^{E}$ | Substrate[c] | | | | Molecule[b] | | |
| | Mg | | O | | C | O | Center of bond |
| Charge (atomic unit) | 1.2 | | −1.2 | | 0.5655268 | 0.2994430 | −0.8649699 |
| Dipole (atomic unit) | 0 | | 0 | | 1.0573340 | −0.4141913 | −0.2865876 |
| Quadrupole (atomic unit) | 0 | | 0 | | −0.2356246 | 0.1296469 | 0.7634119 |

[a]From Ref. 22.
[b]From Ref. 23.
[c]From Ref. 24.

on the internuclear coordinate $Q$. These external and internal dependences occur through $\mathbf{R}$ and $\underline{M}^a$ and the total interaction potential $V$ is thus a function of the coordinates $(x,y,z,\theta,\phi,Q)$ of all the adsorbed molecules,

$$V = V_{\mathrm{MM}}^{\mathrm{DR}} + V_{\mathrm{MS}}^{\mathrm{DR}} + V_{\mathrm{MM}}^{E} + V_{\mathrm{MS}}^{E}. \tag{5}$$

### B. Infrared spectrum

Experimental information on the configuration of the admolecules is partly provided by analysis of the frequency and intensity of the infrared signals, using polarized probe. Since emphasis is not brought to the band shape, we can, therefore, disregard the coupling between the optical $(Q,\theta,\phi)$ and the bath variables ($x,y,z$ and substrate phonons) and limit our study to the bar spectrum. The integrated absorption coefficient for the polarization infrared spectrum is given, within the dipolar approximation, as[6]

$$I_{q_p}(\omega) = \sum_{\gamma} \frac{4\pi}{\hbar c} N \omega E_{\mathbf{q}_p} |\langle 0|Q|1\rangle|^2 \left|\frac{\partial \mu}{\partial Q}\right|^2 \sum_{m=1}^{N_c}\sum_{n=1}^{N_c} c_{\gamma m} c_{\gamma n} \times \sum_{\alpha}\sum_{\beta} e_{m_\alpha} e_{n_\beta} q_{p_\alpha} q_{p_\beta} \delta(\omega-\omega_\gamma), \tag{6}$$

where $N_c$ defines the number of molecules in the primitive cell [$N_c=3$ for the $c(4\times2)$ phase[3,4]] and $N$ is the number of cells in the monolayer. The incident light is characterized by the photon polarization $\mathbf{q}_p$ and the corresponding field intensity $E_{\mathbf{q}_p}$. The expressions for the parallel and perpendicular components $q_{p_\alpha}$ are given in Ref. 10. $\langle 0|Q|1\rangle$ is the fundamental vibrational transition for every CO molecule and $\partial\mu/\partial Q$ the corresponding transition dipole moment.[6] $\mathbf{e}_m(\theta_m,\phi_m)$ defines the orientation of the dipole moment of the $m$th adsorbed CO molecule. The frequencies $\omega_\gamma$ and the coefficients $c_{\gamma m}$ are the eigensolutions of the secular equa-

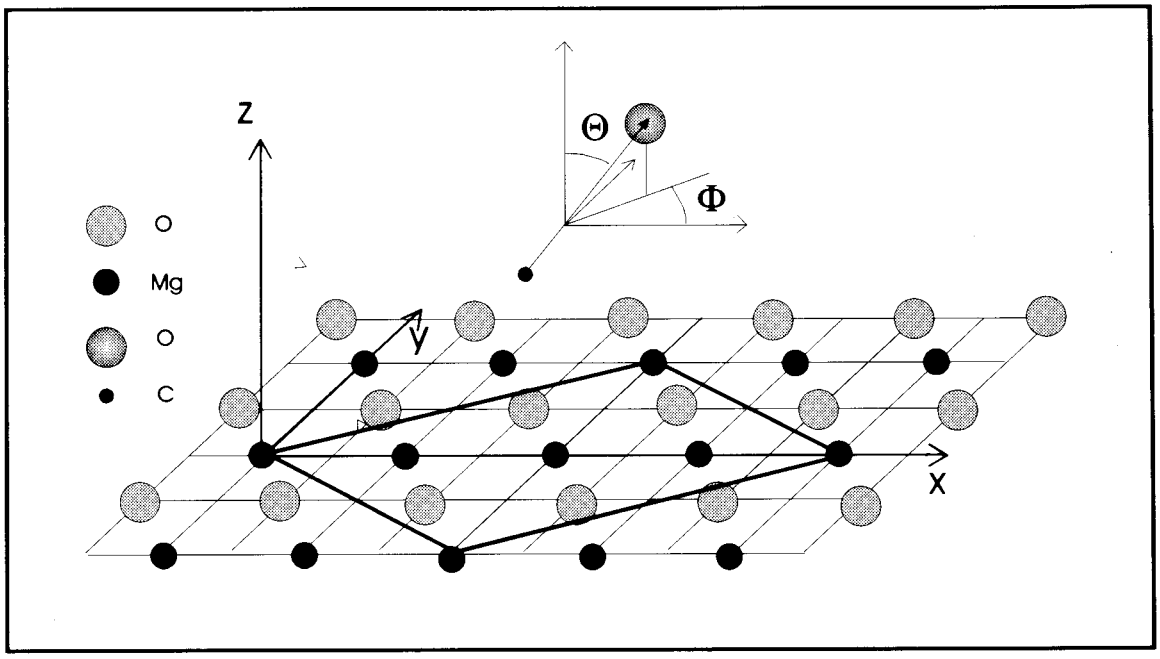


FIG. 1. Geometry of an adsorbed molecule. The CO center of mass position $(x,y,z)$ and orientation $(\theta,\phi)$ are referred to as the absolute frame tied to a cation of the MgO surface. The $c(4\times2)$ primitive cell is also drawn.

tion connected to the internal Hamiltonian of the adsorbed molecules[6,8] when they are assumed to be fixed at their equilibrium orientations.

### C. The monolayer dynamics

Another part of experimental information is brought by the analysis of the orientation-translation dynamics of the monolayer, using HAS results. These external motions are studied by neglecting the dynamical coupling between the monolayer and the substrate. Indeed, it was shown[7] that this coupling does not significantly modify the general shape of the dispersion curves when compared to the uncoupled case, except at the resonances where avoided crossings occur.

The corresponding monolayer Hamiltonian on the rigid substrate is written as[11]

$$H_E=\sum_{\alpha,r,m}\frac{p_\alpha^2\begin{pmatrix} r \\ m\end{pmatrix}}{2A_\alpha}+\sum_{\alpha,r,m}\sum_{\beta,r',m'}\left[\phi_{\alpha\beta}^{\mathrm{MM}}\begin{pmatrix} r & r' \\ m & m'\end{pmatrix}+\sum_{\ell,s,p}\phi_{\alpha\beta}^{\mathrm{MS}}\begin{pmatrix} r & \ell \\ m & sp\end{pmatrix}\delta_{rr'}\delta_{mm'}\right]u_\alpha\begin{pmatrix} r \\ m\end{pmatrix}u_\beta\begin{pmatrix} r' \\ m'\end{pmatrix}, \tag{7}$$

where $u_\alpha\binom{r}{m}$ and $p_\alpha\binom{r}{m}$ are, respectively, the displacement and the momentum associated with the $\alpha$th variable of the $m$th molecule, which pertains to the $r$th primitive cell of the monolayer. $A_\alpha$ represents the molecular mass when $\alpha=x,y,z$ $(A_x=A_y=A_z=4.65\times10^{-23}$ g molecule$^{-1})$, i.e., for the centers of mass oscillations, and the momentum of inertia $I$ or $I\sin^2\theta$ $(I=14.4\times10^{-40}$ g cm$^2$ molecule$^{-1})$, when $\alpha=\theta$ or $\phi$ (Fig. 1), i.e., for the angular librations. $\underline{\phi}^{\mathrm{MM}}$ defines the lateral force constant tensor, which correlates the motions of two molecules and $\underline{\phi}^{\mathrm{MS}}$ describes the holding force constant tensor due to the static substrate.

The dispersion curves which characterize the monolayer dynamics are then obtained by diagonalizing the $(5N_c\times5N_c)$ dynamical matrix $\underline{D}$ connected to the Hamiltonian $H_E$,[11] defined as

$$D_{\alpha\beta}(m,m',\mathbf{q})=\sum_{r'}(A_\alpha A_\beta)^{-1/2}\phi_{\alpha\beta}\begin{pmatrix} r & r' \\ m & m'\end{pmatrix}\times\exp\{-i\mathbf{q}\cdot[\mathbf{R}(r)-\mathbf{R}(r')]\}, \tag{8}$$

where the force constant tensor $\underline{\phi}$ is a contracted notation for $\underline{\phi}^{\mathrm{MM}}$ and $\underline{\phi}^{\mathrm{MS}}$. $\mathbf{q}$ is the two dimensional wave vector, in the plane $(x,y)$ of the layer.

## III. LAYER GEOMETRY THROUGH STATIC CONSIDERATIONS

All theoretical approaches (Hartree-Fock cluster,[12–14] Hartree-Fock periodic,[15] density functional,[16] atom-atom sum[2]) agree that the cation site corresponds to the most stable adsorption site for a single CO molecule, with its axis perpendicular to the surface. When the CO center of mass is shifted with respect to the Mg site along a Mg trough, the molecular axis tends to tilt and it becomes nearly flat above the bridged Mg-Mg site.

At larger coverage, periodic Hartree-Fock calculations showed[15] that the lateral interactions between perpendicular molecules in a $(1\times1)$ structure are repulsive. Atom-atom classical potential calculations[2,6] found a stable $(4\times2)$ phase at 0 K for which the CO centers of mass are aligned along the Mg troughs, forming parallel CO rows mutually shifted along two adjacent troughs. These rows contain three CO molecules spread over four Mg-Mg distances, indicating that the molecules cannot be simultaneously adsorbed on equivalent sites. The conclusions reached by both periodic Hartree-Fock and atom-atom calculations were corroborated by recent periodic pseudopotential results.[17]

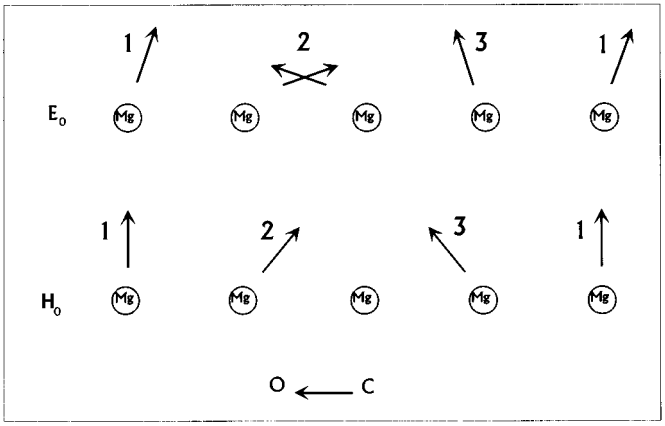


FIG. 2. Geometry of the $c(4\times2)$ CO monolayer adsorbed on MgO(100) for the two configurations $E_0$ and $H_0$ discussed in the text. The circles indicate Mg cations and the arrows CO molecules (side view).

Very recently, we performed[6] atom-atom potential calculations [Eq. (5)] using an improved procedure for the energy minimization and showed that the molecular axes and centers of mass remain confined inside the Mg troughs. These troughs appear as smooth equilibrium valleys for the translational motions along this direction, whereas motions perpendicular to the valleys are relatively hindered. Many of the equilibrium configurations along the valleys were found for the three molecules, which differ by only 1 or 2 meV per molecule. Two sets of configurations arise from a detailed analysis. These two sets differ from the orientation $(\theta,\phi)$ of the three molecules in the primitive cell. In the first set (set $E$, Fig. 2), one molecule lies nearly flat $(\theta_2\simeq70°)$ above the bridge site and the two others lie close to the cation sites, being tilted by $\theta_1\simeq\theta_3\simeq20°$. The absolute minimum $E_0$ is reached when the molecules are collinear to the trough direction $(\phi_i=0$ or $\pi)$. In the second set (set $H$) of stable configurations, one molecule stands upright $(\theta_1=0)$ above a cation, while the other two molecules are shifted with respect to the Mg site and are tilted by $\theta_2\simeq\theta_3\simeq40°$, with $\phi_2=0$ and $\phi_3=\pi$. However, other configurations having $\theta_i$ unchanged, but with molecular axes slightly outside the troughs $(\phi_2=8°,\phi_3=172°)$ have nearly the same energy, although they are less stable than the first set of configurations.

The calculation of the polarization infrared spectrum [Eq. (6)] was then performed[6] on the basis of these static configurations and the result compared to the experimental data. It was shown that the $E$ set of configurations does not explain the observed number of infrared peaks,[5] i.e., three $p$-polarized signals and one $s$-polarized signal. In contrast, the spectrum calculated with the $H$ set of configurations is

TABLE II. Frequencies of the perpendicular mode for the two inequivalent adsorption sites ($i$) of the $c(4\times2)$ phase with the two sets of configurations $E$ and $H$. Experimental values are also given (from Ref. 3).

| | $i$ | $\hbar\omega_z$ (meV) |
|---|---|---|
| $E_0$ | 1 | 10.6 |
| | 2 | 9.0 |
| | 3 | 10.6 |
| $H$ | 1 | 11.3 |
| | 2 | 9.6 |
| | 3 | 9.6 |
| Expt. | twofold degeneracy | 10.5 |
| | no degeneracy | 9.0 |

consistent with the experiments provided that the molecular axes (2) and (3) are rotated by about $\phi_i = 20°$, with respect to the Mg trough. Additional calculations on the structure factor for the two sets $E$ and $H$ are not able to discriminate between the two geometries when compared to LEED experiments.[18] On the basis of these results, we concluded that either potential inaccuracies or finite temperature effects (or both) could favor configurations, which are not found to be the most stable by the optimization procedure at 0 K. Note that the energy difference per molecule for the two sets is about 2 meV, of the order of the thermal energy ($kT \simeq 3.5$ meV at $T = 40$ K), but that it increases significantly when $\phi_i$ deviates by 20° from its equilibrium value.

## IV. INFLUENCE OF MOLECULAR MOTIONS

A more careful examination of the potential energy surfaces experienced by the three molecules in a Mg trough provides additional information that invalidates the previous conclusions. The calculation of the perpendicular frequencies associated with the $z$ motions of the CO centers of mass shows that the value of the frequency is larger when the molecule is closer to the cation site (Table II). In other words, the frequency is maximum above the Mg site, due to the additive influence of the molecule/substrate and lateral interactions, while it is minimum above the bridge site for which the two species of interactions are antagonistic. As a result, the first set (set $E$) of configurations leads to a twofold high frequency mode for the slightly tilted molecules ($i = 1$ and 3) and to a single low frequency mode for the flat molecule ($i = 2$). On the contrary, the second set (set $H$) of configurations leads to the reverse scheme with a twofold degenerate low frequency mode (molecules 2 and 3) and a single high frequency one (molecule 1). Only the first set is consistent with the time of flight data,[3] leading to a close quantitative agreement, whereas the second set, which is suitable for interpreting infrared signals, totally fails (Table II).

To reconcile the two points of view, we study, from Eq. (5), the potential energy maps associated with the other motions ($x$, $y$, $\theta$, and $\phi$) of the three molecules in the neighborhood of the stable configuration $E_0$. First, we find that the $y$ and $\theta$ motions are clearly hindered for every site. These motions are not strongly coupled and they would probably correspond to weakly dispersive frequencies. On the contrary, the $x$ and $\phi$ motions behave very differently

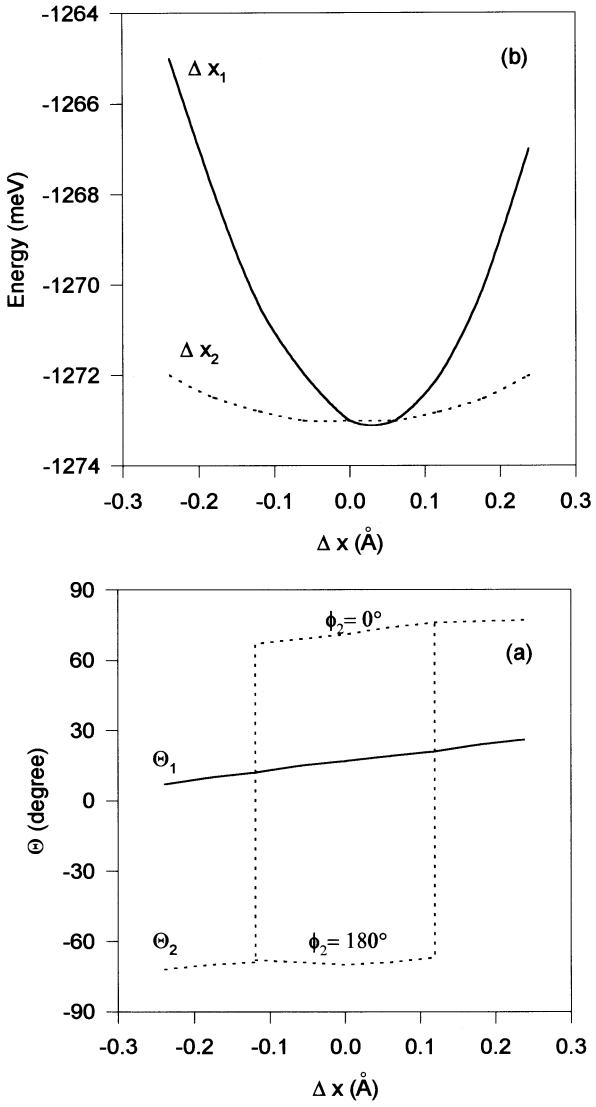


FIG. 3. (a) Orientational configurations for the molecules in the $E_0$ geometry vs the shift $\Delta x_i$ from the equilibrium position along the trough; (b) potential energy curves for the translational motions $\Delta x_i$ parallel to the trough. Note that molecule 3 behaves in the same way as molecule 1.

depending on the molecular site. For the slightly tilted molecules (1 and 3), the $\phi$ barrier although smaller than for the previous motions leads to a spinning hindering. Since the second molecule is flat inside the trough, the $\phi_2$ motion is much more hindered and only 0 or $\pi$ configurations associated with the molecular axis oriented along the trough direction are possible [Fig. 3(a)]. For the translational motions ($x$) along the trough, the two tilted molecules experience a relatively sharp potential well [Fig. 3(b)] due to the lateral interactions, which is reinforced by the surface potential due to adsorption close to the cation. For the nearly flat molecule, the bridge site is less favorable and tends to reduce the well created by the lateral interactions, which appears to be relatively flat.

We can thus schematize the layer dynamics as that of a set of parallel CO chains, each consisting of two molecules undergoing slight linear and angular oscillations about their equilibrium positions ($i = 1$ and 3), on each side of a third molecule ($i = 2$) performing large amplitude linear oscilla-

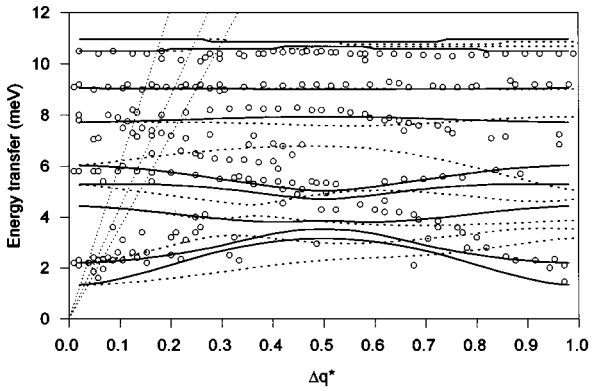


FIG. 4. Comparison between the calculated dispersion curves (solid lines) for the $E_0$ geometry and the experimental data (circles) from HAS inelastic measurements at $T=36$ K. The full and broken curves correspond to the layer domain for which the CO rows are along the $x$ and $y$ directions, respectively. The three dotted lines represent the bulk and Rayleigh modes of the substrate.

tions along the troughs (Fig. 3). The axis of this latter molecule librates around the equilibrium value $\theta_2 \simeq 70°$, while the $\phi_2$ motion is coupled to the $x_2$ motion. When the molecular center of mass remains confined close to the bridge site ($-0.12$ Å $\leqslant \Delta x_2 \leqslant 0.12$ Å), the CO axis takes indifferently the $\phi_2=0$ or $\pi$ orientations. For larger $\Delta x_2$ values, the CO axis points towards the left or right molecules ($i=1,3$), depending on the sign of $\Delta x_2$ [Fig. 3(a)]. The $\phi_2$ barrier is clearly large, since the axis is confined inside the trough, and in a classical interpretation, the flip-flop motion ($\phi_2=0 \rightleftharpoons \pi$) can only be favored by a simultaneous increase of the molecule/surface distance.

A further examination of the influence of the lateral interactions on the molecular motions shows that the total energy per molecule is quite independent of the $\phi_2$ orientation ($\phi_2=0$ or $\pi$). The molecules $i=2$ can, therefore, be indifferently oriented collinear or antilinear to the CO chains, the flip-flop motion being possible, from the quantum mechanical point of view, through the coupling with the translation, as a tunneling mode.

## V. INTERPRETATION OF THE EXPERIMENTAL DATA

Within the scheme of the CO layer geometry viewed as a set of parallel CO lines formed by 2 slightly tilted molecules and one indifferently oriented collinear or antilinear nearly flat molecule (Fig. 2), we calculate the characteristics measured by HAS (Ref. 3) and PIRS (Refs. 4,5) Note that we must account for the possibility of having two perpendicular domains, for which the CO lines are parallel to the $x$ or $y$ directions, respectively. Indeed both the PIR spectrum and HAS dispersion curves are sensitive to this feature.

The dispersion curves $\hbar\omega(\Delta q)$ for the external vibrations of the $c(4\times2)$ CO monolayer containing the three molecules per primitive cell and defined by their equilibrium configuration $E_0$ (Fig. 2) are shown in Fig. 4. These curves are calculated by solving the dynamical matrix of the monolayer adsorbed on the rigid substrate [Eq. (8)]. We consider the two possibilities for molecule (2) involving the flip-flop motion. Moreover, we have superimposed the bulk and Rayleigh frequency curves[19] of the substrate on those of the layer. Among the 15 dispersion curves expected for each monolayer domain, 9 occur at energies lower than 12 meV. The four high frequency dispersionless modes at 10.5–10.9 meV and the two modes at 9 meV are clearly assigned to layer motions perpendicular to the surface. Due to the small splitting, the highest modes, which correspond to the two tilted molecules 1 and 3, appear to be twofold degenerate with respect to the lower mode for each domain. The medium frequency modes between 6 and 8 meV are more dispersive; they characterize mainly motions parallel to the surface and describe the coupling between $\phi_i$ librations and $y_i$ translations (perpendicular to the trough). The low frequency modes below 5 meV are assigned to $y_i$ translations and to couplings between $x_i$ translations and $\theta_i$ librations. These low frequency modes are not pure and they show moreover energy gaps at $\Delta q=0$. Around 1 meV, the gap characterizes the $(\theta_i, x_i)$ corrugation along the Mg troughs, while around 2 meV it describes the corrugation perpendicular to these troughs.

The general scheme of dispersion curves agrees satisfactorily with the point data recorded from time of flight spectroscopy.[3] The consistency is quite good for the frequency modes at 6 and 8 meV and especially for the most intense perpendicularly polarized modes at 9 and 10.5–10.9 meV. The energy gap for the low energy dispersion curves is also well reproduced.

Six other dispersion curves with parallel polarization occur furthermore at frequencies higher than those considered in Fig. 4: four more-or-less dispersive modes in the range 19–22 meV characterize mainly angular $(\theta_i, \phi_i)$ couplings between the two tilted molecules 1 and 3 ; two dispersionless modes around 15–16 meV correspond to mixing of angular and linear oscillations of the nearly flat molecule 2. However, these six curves have not been observed within the experimental conditions.[3]

The polarization infrared spectrum [Eq. (6)] is significantly modified when compared to the static situation,[6] because polarized photons probe the average geometry of the layer. For molecules 1 and 3, nothing is changed since they give rise to the $p$ and $s$ signals calculated previously; in contrast, only the perpendicular component of the second molecule dipole is probed by the photons after averaging over the two equivalent collinear and antilinear configurations. Consequently, three signals occur for the $p$-polarized spectrum, which are split by the vibrational coupling between molecules and a single $s$ peak is calculated, which is due to the out-of-phase vibration of the tilted molecules. Such a result is quite consistent with the experiments,[4,5] as shown in Fig. 5, given the inaccuracies inherent to the vibrational dependence of the interaction potential.

In passing, note that the $c(4\times2)$ geometry assigned by experiments is not strictly valid in the sense that the orientation of the molecules 2 in the layer is not defined, being either collinear or antilinear. Both LEED and HAS probes cannot discriminate the two orientations and the resulting assignment does not take into account this ambiguity. In contrast, polarization infrared spectroscopy could, in principle, discriminate structures formed by domains with only collinear molecules from those with only antilinear molecules. Such an event would occur for long range correlated molecules through lateral interactions. The fact that infrared is

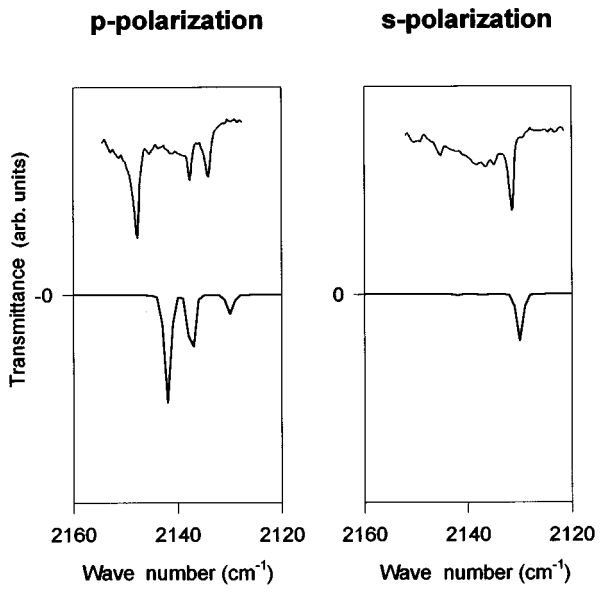


FIG. 5. Polarization infrared spectrum for the dynamical $E_0$ configuration. Comparison between the experimental spectrum recorded at 35 K and the calculated one, convoluted with a Lorentzian shape (full width at half maximum of 1.1 $cm^{-1}$). The fact that the base line is not zero for the experimental spectrum is due to additional inhomogeneous mechanisms.

unable to see such a feature seems to corroborate our findings on the random distribution of dynamical dipoles.

A second remark concerns the influence of temperature on HAS and infrared signals. Above 50 K, experiments display a phase transition from the $(4\times2)$ geometry towards a less dense $(1\times1)$ structure. This result is again consistent with our dynamical model, which shows that the $\phi$ barriers for the tilted molecules (1 and 3) are relatively small. Increasing temperature up to 50 K will result in a free spinning of these molecules, while the $\theta$ motions remain librational. The *p*-polarized photons will thus be sensitive to the perpendicular components of the dynamical dipoles, whereas the *s* component will vanish after averaging. The resulting spectrum will be characterized by perpendicular signals only. Further, averaging over $\phi_i$ ($i=1$ and 3) will lead to a vanishing dipolar coupling between molecules, yielding a single threefold degenerate *p* peak in the spectrum, in agreement with infrared experiments. Concerning the single dispersion curve observed around 9.5 meV for the high temperature $(1\times1)$ phase, the less dense structure tends to favor uncorrelated motions inside the Mg troughs, due to the decrease of the lateral interaction influence.[6] The existence of rows is corroborated by LEED experiments,[2] which show the occurrence of $(n\times2)$ structures beyond 50 K. The randomization of the centers of mass positions along the troughs will then result in an averaging of the perpendicular vibrational mode frequency.

Finally, we point out that such a model is not specific to CO adsorbed on MgO (001). Other substrates, such as dielectrics [NaCl (Ref. 20)] or metals [Cu(110) (Ref. 21)] exhibit flat equilibrium valleys, which behave as troughs for adsorbed atoms or molecules. We, thus, expect to recover a similar ambiguity on the assignment of the adlayer structures implying molecular orientations.

## ACKNOWLEDGMENTS

The Laboratoire de Physique Moléculaire is ''Unité associée au Centre National de la Recherche Scientifique No. 772.''

[1] P. Audibert, M. Sidoumou, and J. Suzanne, Surf. Sci. Lett. **273**, L467 (1992).
[2] V. Panella, J. Suzanne, P.N.M. Hoang, and C. Girardet, J. Phys. (France) I **4**, 905 (1994).
[3] R. Gerlach, A. Glebov, G. Lange, J.P. Toennies, and H. Weiss, Surf. Sci. **331-333**, 1490 (1995).
[4] J. Heidberg, L. Cabigon, E. Kampshoff, M. Kandel, R. Kühnemuth, D. Meine, B. Redlich, O. Schönekäs, M. Suhren, H. Weiss, and D. Wetter, in *Adsorption on Ordered Surfaces of Ionic Solids and Thin Films*, edited by H.J. Freund and E. Umbach (Springer, Berlin, 1993), p. 46.
[5] J. Heidberg, M. Kandel, D. Meine, and U. Wild, Surf. Sci. **331-333**, 1467 (1995).
[6] P.N.M. Hoang, S. Picaud, and C. Girardet Surf. Sci. (to be published).
[7] C. Girardet, C. Ramseyer, P.N.M. Hoang, and S. Picaud, Phys. Rev. B **52**, 2144 (1995).
[8] S. Picaud, S. Briquez, A. Lakhlifi, and C. Girardet, J. Chem. Phys. **102**, 7229 (1995).
[9] S.L. Price, A.J. Stone, and M. Alderton, Mol. Phys. **52**, 987 (1984).
[10] S. Briquez, A. Lakhlifi, S. Picaud, and C. Girardet, Chem. Phys. **194**, 65 (1995).
[11] S. Picaud, P.N.M. Hoang, and C. Girardet, Surf. Sci. **322**, 381 (1995).
[12] G. Pacchioni, G. Cogliandro, and P.S. Bagus, Surf. Sci. **255**, 344 (1991).
[13] M.A. Nygren, L.G.M. Petterson, Z. Barandiaran, and L. Seijo, J. Chem. Phys. **100**, 2010 (1994).
[14] J.A. Mejias, A.M. Marquez, J. Fernandez Sanz, M. Fernandez Garcia, J.M. Ricart, C. Sousa, and F. Illas, Surf. Sci. **327**, 59 (1995).
[15] R. Dovesi, R. Orlando, F. Ricca, and C. Roetti, Surf. Sci. **186**, 267 (1987).
[16] K.M. Neyman and N. Rösch, Chem. Phys. **177**, 561 (1993).
[17] C. Minot, M.A. Van Hove, and J.P. Biberian, Surf. Sci. **346**, 283 (1996).
[18] J. Suzanne (private communication).
[19] W. Kress, in *Surface Phonons*, edited by W. Kress and F.W. de Wette (Springer, Berlin, 1991), p. 209.
[20] C. Ramseyer and C. Girardet, J. Chem. Phys. **103**, 5767 (1995).
[21] P. Zeppenfeld, M. Büchel, R. David, G. Comsa, C. Ramseyer, and C. Girardet, Phys. Rev. B **50**, 14 667 (1994).
[22] A. Lakhlifi and C. Girardet, Surf. Sci. **241**, 400 (1991).
[23] S. Picaud, P.N.M. Hoang, C. Girardet, A. Meredith, and A.J. Stone, Surf. Sci. **294**, 149 (1993).
[24] M. Sidoumou, V. Panella, and J. Suzanne, J. Chem. Phys. **101**, 6338 (1994).